CrossMark

Regional groundwater flow and geochemical evolution in the Amacuzac River Basin, Mexico

Eric Morales-Casique[1] · Jacobo Guinzberg-Belmont[2] · Adrián Ortega-Guerrero[3]

Abstract An approach is presented to investigate the regional evolution of groundwater in the basin of the Amacuzac River in Central Mexico. The approach is based on groundwater flow cross-sectional modeling in combination with major ion chemistry and geochemical modeling, complemented with principal component and cluster analyses. The hydrogeologic units composing the basin, which combine aquifers and aquitards both in granular, fractured and karstic rocks, were represented in sections parallel to the regional groundwater flow. Steady-state cross-section numerical simulations aided in the conceptualization of the groundwater flow system through the basin and permitted estimation of bulk hydraulic conductivity values, recharge rates and residence times. Forty-five water locations (springs, groundwater wells and rivers) were sampled throughout the basin for chemical analysis of major ions. The modeled gravity-driven groundwater flow system satisfactorily reproduced field observations, whereas the main geochemical processes of groundwater in the basin are associated to the order and reactions in which the igneous and sedimentary rocks are encountered along the groundwater flow. Recharge water in the volcanic and volcano-sedimentary aquifers increases the concentration of HCO_3^-, Mg^{2+} and Ca^{2+} from dissolution of plagioclase and olivine. Deeper groundwater flow encounters carbonate rocks, under closed CO_2 conditions, and dissolves calcite and dolomite. When groundwater encounters gypsum lenses in the shallow Balsas Group or the deeper Huitzuco anhydrite, gypsum dissolution produces proportional increased concentration of Ca^{2+} and SO_4^{2-}; two samples reflected the influence of hydrothermal fluids and probably halite dissolution. These geochemical trends are consistent with the principal component and cluster analyses.

Keywords Mexico · Regional groundwater flow · Hydrogeochemistry · Principal component analysis · Geochemical modeling

✉ Eric Morales-Casique
  ericmc@geologia.unam.mx

[1] Instituto de Geología, Universidad Nacional Autónoma de México, C.P. 04510 México, D.F., Mexico

[2] Superintendencia de Estudios Zona Pacífico Norte, Comisión Federal de Electricidad, C.P. 44870 Guadalajara, Jalisco, Mexico

[3] Centro de Geociencias, Universidad Nacional Autónoma de México, C.P. 76230 Querétaro, Mexico

Introduction

Understanding the regional hydrogeologic system is important for water resources management in hydrologic basins. Regional analysis requires basin-scale characterization of the groundwater flow pattern and provides a hydrogeologic framework to analyze geologic and geochemical process (Tóth 1995, 1999; Garven 1995; Pearson et al. 1996). Basin-scale flow analysis recognizes that all geologic formations are permeable to some degree and that at appropriate time and length scales, they form a hydrologic continuum (Tóth 1995). In addition, regional characterization of the flow pattern defines a conceptual-mathematical model of the hydrogeologic system that can be used as a framework for local and more detailed studies and to define regional boundaries (Ortega and Farvolden 1989).

Numerical modeling is a very useful tool in implementing and testing quantitatively a conceptual model; however, a fully three-dimensional (3D) basin-scale model requires large quantities of data and can be computationally expensive. A useful and more economical alternative is to model selected two-dimensional (2D) cross-sections of the system. Tóth

(1963) developed an analytical solution to the cross-sectional, regional flow problem in an idealized basin and pointed to the nested organization of the groundwater flow pattern into flow systems ranging from local to regional. Freeze and Witherspoon (1966, 1967, 1968) employed numerical modeling to investigate the resulting groundwater flow pattern for different water-table configurations and contrasting hydraulic conductivities in a synthetic stratigraphy. There have been several improvements and applications to 2D cross-section regional groundwater-flow modeling such as coupling fluid flow and heat flow (Forster and Smith 1988a, b), correlating the flow pattern with geochemical data (Ortega-Guerrero 2003), simulation of brine migration (Deming and Nunn 1991) and simulation of the genesis of mineral deposits (Garven and Freeze 1984a, b; Garven et al. 1993).

Geochemical data of groundwater pose additional constraints that are correlated to groundwater flow pattern and help to condition the conceptual model. Typically, groundwater in sedimentary rocks will exhibit trends in chemical composition that correlate with the length of the flow path. Among the trends along the direction of groundwater flow are: from low to elevated pressure and temperatures, from strong to no fluctuations in water quality, from acidic to basic, from oxic to anoxic–methanogenic, from no to significant base exchange, and from fresh to brackish (Stuyfzand 1999). However, the chemical composition of groundwater may vary for similar flow lengths depending on the order in which the various sedimentary strata are encountered by the groundwater and the partial pressure of the CO_2 in the soil zone (Palmer and Cherry 1984).

An approach is presented for hydrogeologic characterization that integrates geologic, hydrologic and geochemical data to postulate a conceptual-mathematical model of regional groundwater flow in the Amacuzac River Basin. The strengths of numerical and geochemical modeling plus multivariate statistical analysis are combined to support the conceptual model. The approach relies on cross-sectional numerical analysis of steady-state groundwater flow to characterize the flow pattern, principal component and cluster analyses of chemical data to identify and postulate geochemical processes and equilibrium geochemical modeling to compute saturation indexes. The aim is to illustrate how groundwater flow modeling and multivariate statistical analysis can add value to the geochemical analysis using traditional techniques. Among the key elements of the conceptual model are: recharge rates, discharge to the Amacuzac River, estimates of regional values of hydraulic conductivity, the groundwater flow pattern through a complex arrangement of volcanic, volcano-sedimentary and carbonate rocks and the main geochemical processes that influence the chemical characteristics of groundwater in the basin.

Hydrogeologic background of the Amacuzac River Basin

The basin of the Amacuzac River (ARB) is located south of the Basin of Mexico, where Mexico City is built, and the Basin of the Lerma River (Fig. 1) and has an area of 9,470 km^2. Annual pluvial precipitation is greatly influenced by topography, ranging from about 1,500 mm on the mountainous north portion of the basin to 800 mm or less in the lower elevation valleys in the southern part.

The ARB develops in the paleogeographic element of the Guerrero-Morelos platform, and the basement of the ARB is a Mesozoic low-grade metamorphic unit (Nieto-Samaniego et al. 2006). The most characteristic rocks of the Guerrero-Morelos platform are a thick succession of marine strata of the Morelos and Cuautla formations (Albian-Maastrichtian; DeCerna et al. 1980; Hernández-Romano et al. 1997). This
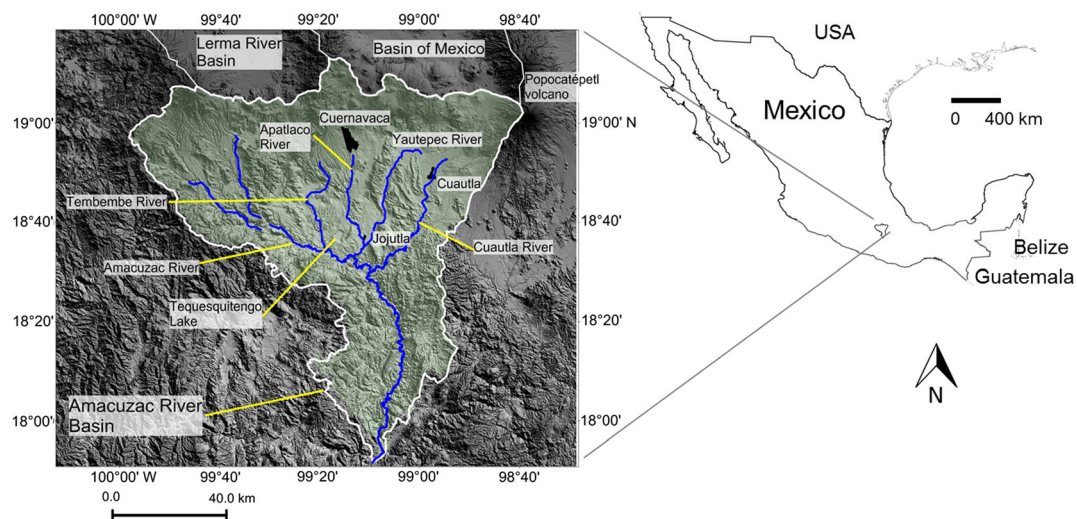

Fig. 1 The basin of the Amacuzac River

marine succession is made up of shallow marine limestone that grades upwards to Turonian–Campanian pelagic limestone and siliciclastic of the Mexcala Formation (Hernández-Romano et al. 1997; Aguilera-Franco 2003).

Based on the hydrogeologic behavior of the rocks within the basin, they were grouped into six main hydrostratigraphic units (Fig. 2). The oldest hydrogeologic unit (HU-0) is a low-grade metamorphic Jurassic basement (Nieto-Samaniego et al. 2006), considered as an aquitard. Overlying the metamorphic basement is a Cretaceous aquifer (HU-1). This integrates a series of permeable formations (Zicapa, Huitzuco, Xochicalco, Morelos and Cuautla), which forms most of the basin and its maximum thickness surpasses 1,000 m (Fries 1960, 1965); this aquifer also exhibits evidence of karst development such as dolines, caves, sinkholes and large-flow springs. The Zicapa Formation is formed by red beds with intercalated beds of marine limestone (Aptian-Albian), in the eastern part of the ARB, whereas in the western part of the ARB, the Zicapa Formation is absent and the lower unit is the Huitzuco anhydrite (DeCerna et al. 1980; Nieto-Samaniego

et al. 2006), followed by karstic, Lower Cretaceous limestones corresponding mainly to Xochicalco and Morelos formations (Fries 1960, 1965). Overlying the carbonate aquifer (HU-1), there is an aquitard (HU-2), which groups the Mexcala Formation and the Balsas Group; the Mexcala Formation (Upper Cretaceous) is constituted by alternated marine beds of sandstone, siltstone and shale, while the Tertiary Balsas Group unconformably overlies deformed beds of the Morelos and Mexcala formations and groups a variety of lithologies—mainly conglomerate, sandstone, siltstone and gypsum lenses—with thicknesses from a few centimeters up to 30 m (Fries 1960, 1965); Fries (1960) postulates that the gypsum lenses were originated from erosion of areas where the Lower Cretaceous anhydrite was exposed. An aquitard in volcanic rocks of the Tertiary (HU-3), including the Tlaica Formation and the Tilzapotla Rhyolite (Fries 1965), overlies aquitard HU-2. An aquifer in volcano-sedimentary rocks of the Tertiary-Quaternary (HU-4), which groups the Cuernavaca and Tlayecac formations and other alluvial deposits, overlies the volcanic aquitard HU-3. The youngest


Fig. 2 Hydrogeologic units
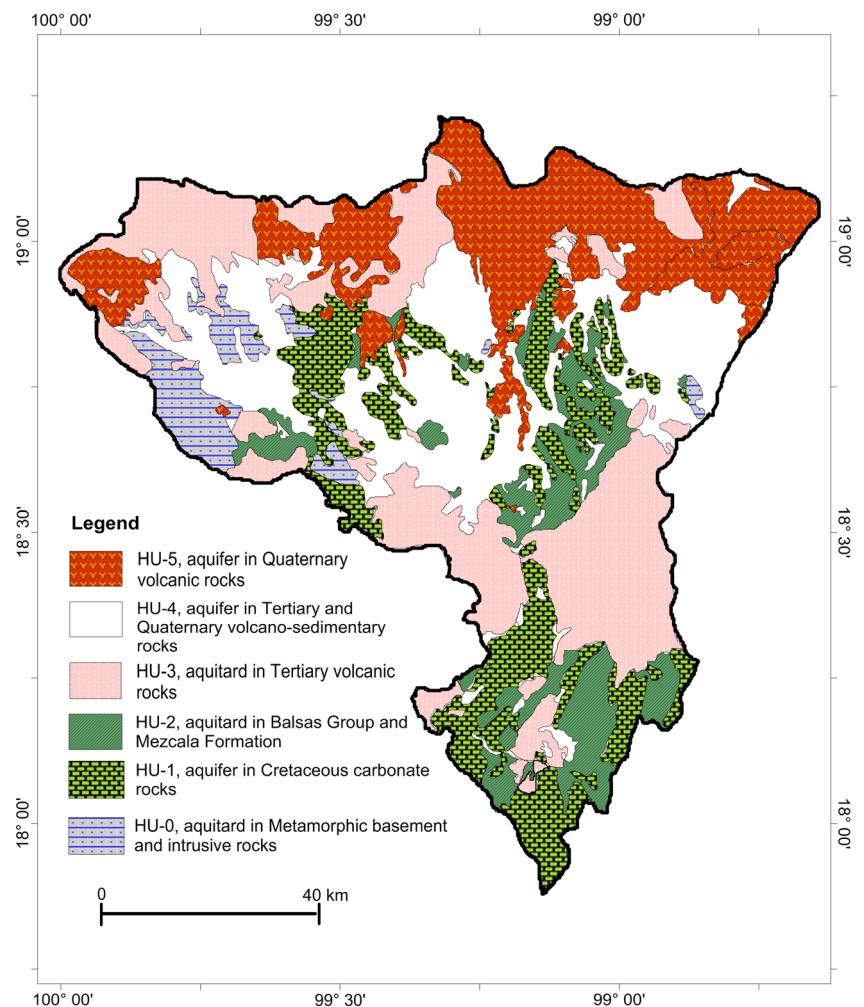
hydrogeologic unit corresponds to an aquifer in Quaternary volcanic rocks (HU-5), including the basaltic rocks and pyroclastics of the Chichinautzin Group (Fries 1960, 1965).

Figure 3 depicts a plain view of the groundwater flow pattern in the three main valleys of the basin (Secretaría de Agricultura y Recursos Hidráulicos 1981a, b, c). Groundwater flow direction is predominantly N–S in the central portion of the basin and N–SW in the eastern portion. The lower elevation valleys are characterized by shallow water table, springs and artesian wells. Groundwater development has not distorted the natural flow patterns in the aquifers of the basin (reports on groundwater availability by aquifer in Mexico, CONAGUA 2015), which supports the assumption that in the long term there exists a dynamic equilibrium between inputs and outputs. Few data are available to infer the position of the regional water table in the mountains. Ortega and Farvolden (1989) report a well in the Sierra Chichinautzin with a water-table elevation of about 2,500 masl, 250 m below the ground surface; this suggests a minimum value for the elevation of the groundwater divide between the Basin of Mexico and the ARB (Fig. 1). In addition, the presence of perennial springs located at about 2,600 masl suggests this value is a lower bound to the elevation of the groundwater divide between the basins of the Amacuzac River and the Lerma River (Fig. 1).

Hydraulic conductivity values, obtained from pumping tests in the volcano-sedimentary aquifers (HU-4), range from 0.01 to more than 200 m/day (Secretaría de Agricultura y Recursos Hidráulicos 1981a, b, c); however, there is no information from pumping tests for the rest of the hydrogeologic units. Via numerical modeling of regional steady-state groundwater flow, Ortega and Farvolden (1989) estimated values of hydraulic conductivity for the hydrogeologic units of the Basin of Mexico (Fig. 1), which correlate with some of the hydrogeologic units in the ARB. They estimated 0.86 m/day for HU-1, 0.0086 m/day for HU-3, 4.3 m/day for HU-4 and 0.43 m/day for HU-5. Bendig (1995) simulated groundwater flow in a region near Cuernavaca and estimated 0.086 m/day for HU-1, 4.3 m/day for HU-4 and 0.09 m/day for HU-5.

Fig. 3 Groundwater equipotentials (*red*), main rivers (*blue*) modeling sections and location of sampled points
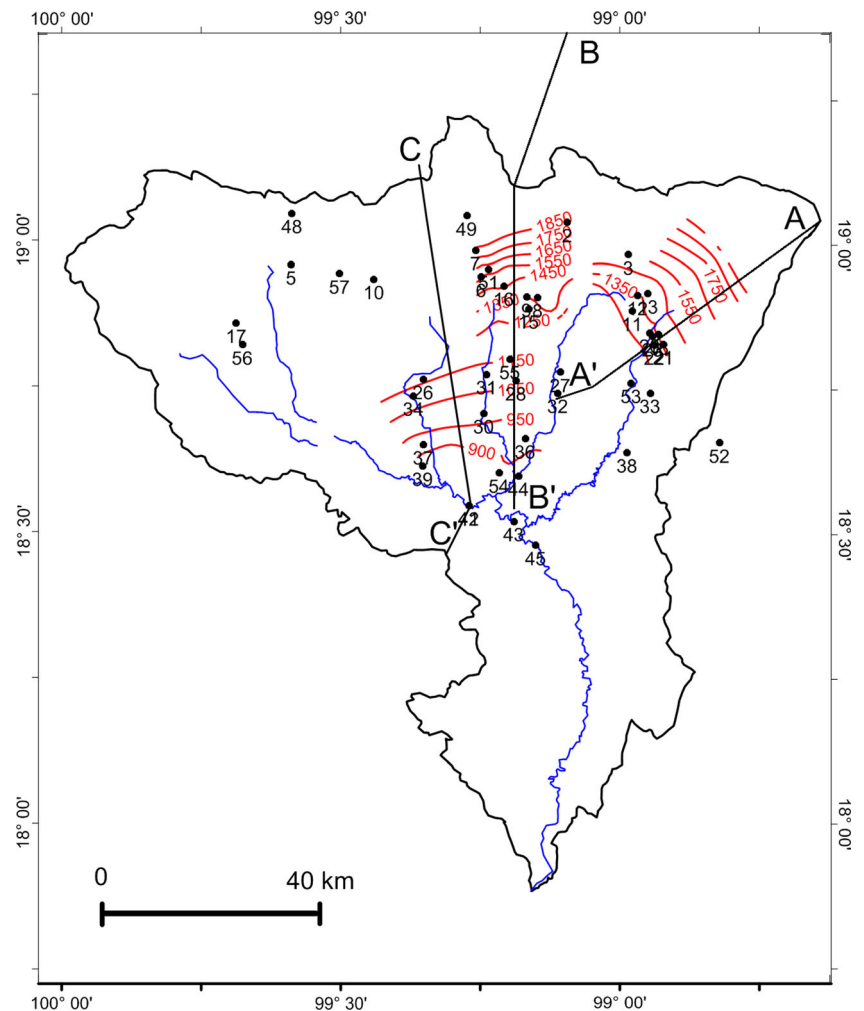
Materials and methods

Groundwater flow modeling

It is assumed that the flow system is driven by gravity, that there are not density effects, and that at the basin scale there exists a dynamic equilibrium between inputs and outputs such that the flow system can be approximated by a steady-state flow field. Under these assumptions, the equation governing the distribution of hydraulic head h is

$$\nabla \cdot (\mathbf{K} \nabla h) = 0 \qquad (1)$$

and depends only on the hydraulic conductivity tensor $\mathbf{K}$ of each hydrogeologic unit. It is further assumed that $\mathbf{K}$ is homogeneous within each hydrogeologic unit with principal directions aligned with the axis of coordinates, which renders $\mathbf{K}$ diagonal, and that at the regional scale both fractured and karstic media can be approximated by equivalent porous media. Long et al. (1982) determined that fracture systems behave more like porous media when (1) fracture density is increased, (2) apertures are constant rather than distributed, (3) orientations are distributed rather than constant, and (4) larger sample sizes are tested. Scanlon et al. (2003) and Ghasemizadeh et al. (2015) have shown the ability of equivalent porous media models to simulate regional groundwater flow in karstified aquifers. These requirements are probably met, given the scale of tens of kilometers of this study and the fracturing due to the intense tectonic evolution of this region of Mexico (Nieto-Samaniego et al. 2006). The flow equation is solved numerically using the code CROSSFLO (McLaren 1988) which solves the 2D flow problem in terms of h and the stream function ψ based on the dual formulation of Frind and Matanga (1985).

Three cross sections approximately parallel to the direction of groundwater flow were selected (Fig. 3): section AA′, Popocatépetl-Cuautla-Las Estacas, of 60 km length; section BB′, Basin of Mexico-Chichinautzin-Cuernavaca-Amacuzac River, of 92 km; and section CC′, Zempoala-Tequesquitengo-Amacuzac River, of 76 km. Section AA′ ends at the spring Las Estacas because this area has been suggested as the discharge area of the Cuautla Aquifer (Comisión Nacional del Agua 1989; Niedzielski 1994) and because in this region the flow pattern converges towards section BB′. Section BB′ was prolonged about 30 km into the Basin of Mexico to investigate the position of the groundwater divide between both basins. Figure 4 depicts the hydrostratigraphy for each section and the boundary conditions for the simulations. Lateral and lower boundaries are no flow boundaries ($\psi = 0$); the elevation of the lower boundary was fixed at sea level. The elevation of the water table is specified based on available piezometric data, while at the mountains the upper boundary condition was set to a free surface with a given recharge rate (defined

as a percentage of the annual precipitation). Each section was discretized into at least 1,900 triangular elements. The simulation strategy was similar to that used by Jamieson and Freeze (1983) and Ortega and Farvolden (1989). The simulation was started by using values of hydraulic conductivity and recharge rates suggested by previous studies (Ortega and Farvolden 1989; Bendig 1995) and the average of the pumping tests in HU-4. In general, there exists a nonunique relation between flux (recharge) at the boundary and $\mathbf{K}$ of the hydrogeologic units. To further constrain the relation between flux and hydraulic conductivity, three natural conditions were imposed. Firstly, the water table at the mountains cannot be consistently higher than topography. Secondly, its elevation cannot be too low either because this would not be consistent with the existence of some springs and the lone water-table measurement available (2,500 masl). The third natural constraint is that flux at the boundary cannot be larger than the mean annual precipitation. Values of hydraulic conductivity and recharge rate were adjusted to comply with the natural constraints, to reach a reasonable position of the water table in the mountains and reproduce the general characteristics of the discharge pattern to springs and rivers in the basin.

Once the groundwater flow net is computed, residence time in the saturated zone can be estimated from a stream tube using (Frind and Matanga 1985)

$$t = \frac{1}{\Delta\psi} \sum_j \phi_j A_j \qquad (2)$$

where ϕ and A are respectively effective porosity and partial area of the stream tube corresponding to the j-th hydrogeologic unit, and ψ is the stream function so that $\Delta\psi = \psi_2 - \psi_1$ is the specific discharge of the stream tube. The estimate provided by Eq. (2) assumes piston flow in a steady-state flow field. An estimate with less uncertainty would involve solving an equation for the cumulative distribution function of residence time under transient flow conditions and accounting for climatic variations, dispersion, matrix diffusion and heterogeneity within the hydrogeologic units (Varni and Carrera 1998; Weissmann et al. 2002).

Groundwater sampling and chemical analysis

Forty-five locations were sampled throughout the basin for chemical analysis of major ions (Fig. 3). Of these locations, 26 correspond to springs, 16 are deep wells and 3 were taken from rivers. Sample points were selected taking into account the groundwater flow pattern and the three cross sections in Fig. 3. Electrical conductivity (EC), temperature, pH and total alkalinity (by titration using a bromocresol green indicator solution) were measured in the field and samples were stored at 4 °C. Major ions were analyzed at the Analytic Chemistry
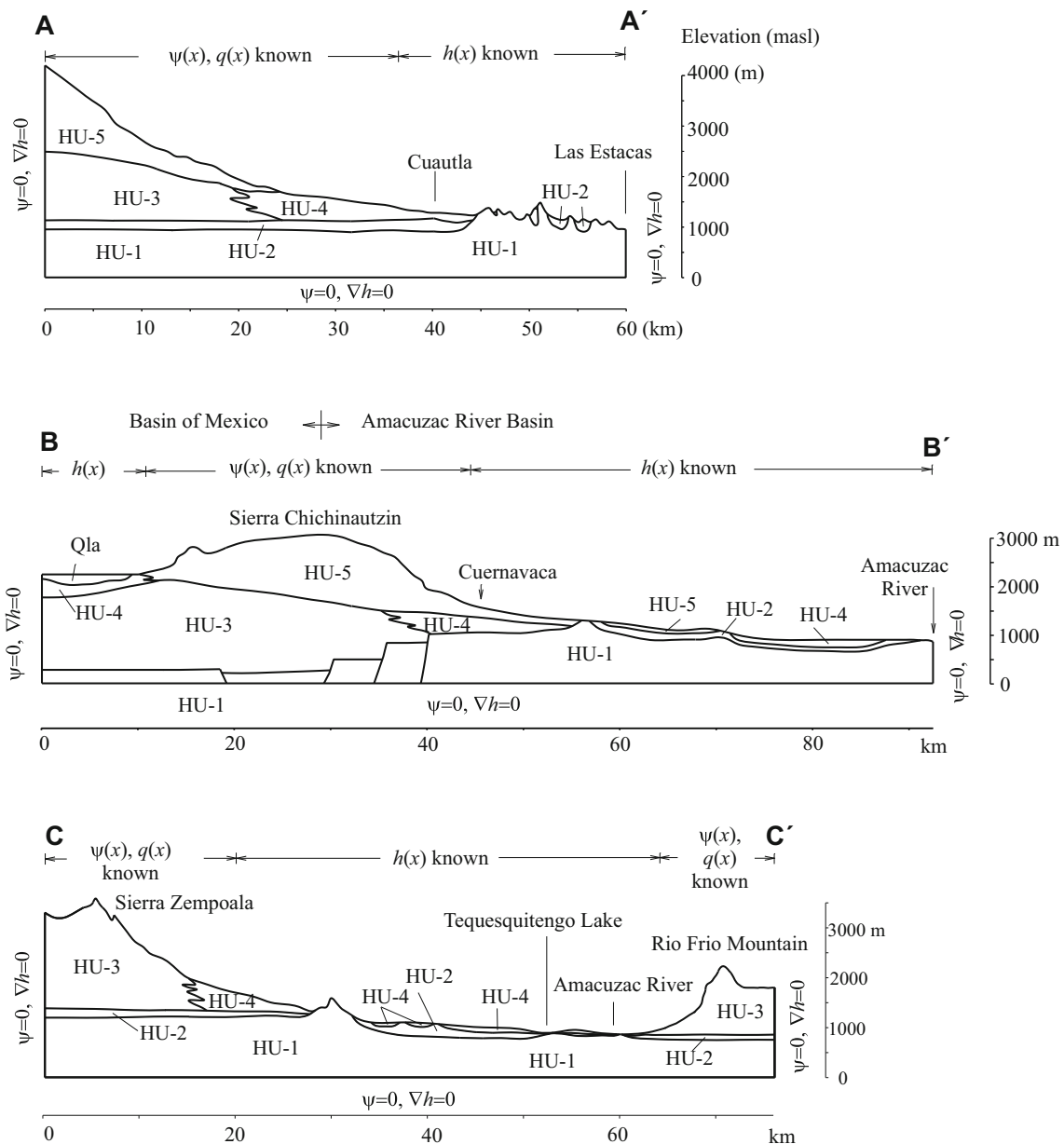
Fig. 4 Modeling sections AA', BB', CC': hydrostratigraphy and boundary conditions

Laboratory of the Geology Institute at UNAM (National Autonomous University of Mexico).

Multivariate statistical analysis

Principal component analysis, PCA (Everitt and Hothorn 2010) is employed as a diagnostic tool to detect trends in the geochemical data. PCA is based on eigenvalue analysis of a $n \times p$ correlation matrix of chemical composition, where n is the number of samples and p is the number of chemical species. The eigenvectors of the correlation matrix form a new orthogonal system of coordinates known as the principal components (pc) of the data set. The first eigenvector (pc1) is aligned with the direction of largest variance in the data set.

The second eigenvector (pc2) is aligned with the direction of the second largest variation in the data set, and so on. Typically, the first two or three eigenvectors explain close to 90 % of the variability in a data set; hence, PCA can be used as a tool to reduce the dimensionality of a large data set and to find patterns in complex systems. PCA has been successfully applied for interpreting hydrologic processes through the analysis of large hydrogeochemical data sets (Christophersen and Hooper 1992; Laaksoharju et al. 1999; Hooper 2009).

After PCA, samples with similar chemical characteristics are grouped by hierarchical cluster analysis. Clusters are generated based on the scores obtained from PCA to avoid the inclusion of mutually dependent variables (Suk and Lee 1999; Long and Valder 2011). The number of clusters is obtained by

hierarchical clustering (Ward 1963) and selected based on calculated probability values (p-values) for each cluster using bootstrap resampling techniques (Suzuki and Shimodaira 2006).

Geochemical modeling

Geochemical modeling was conducted to identify minerals that are in equilibrium with sampled groundwater and to relate groundwater composition to the hydrogeologic units that it encounters along flow paths. Saturation indexes with respect to gypsum, anhydrite, dolomite and calcite were computed using the code PHREEQE (Parkhurst et al. 1980). The partial pressure of CO_2 (P_{CO2}) was computed assuming a closed system.

Results and discussion

Groundwater flow modeling

Flow patterns

Table 1 presents the estimated values of **K** for each hydrogeologic unit. Estimated values of K_h for aquifers range from 0.4 m/day (HU-5) to 2 m/day (HU-4), while values for aquitards range from 0.005 m/day (HU-3) to 0.01 m/day (HU-2). The ratio of K_h/K_v was estimated as 10 except for HU-3 and HU-4, which had a value of 5. These values represent effective parameters assuming that each hydrogeologic unit is homogeneous, provide an estimate of the mean value within each unit and are supported in qualitative terms by the fact that the flow and discharge pattern agree with the hydrologic evidences at the basin scale. Based on a sensitivity analysis (not shown), the three natural constraints mentioned in section 'Groundwater flow modeling' allow for the estimation of **K** within an order of magnitude. Modeling results were particularly sensitive to **K** of HU-1; increasing **K** by an order of magnitude leads to a flat water table, while decreasing it by one order of magnitude leads to a water table considerably higher than topography of the mountain ranges.

Figure 5 depicts the simulated flow pattern and the computed fluxes at the water table for the three selected sections.

Recharge rates were estimated at 35–50 % of the annual precipitation. Higher rates produce a water-table elevation above the topography, while recharge rates lower than 25 % result in the neighboring north basins draining towards the Amacuzac River Basin. In section AA′ (Fig. 5), 35 % of the pluvial precipitation infiltrates in the broad volcanic and volcano-sedimentary fan from the slopes of the Popocatepetl Volcano to the city of Cuautla. With respect to discharge, 60 % of it occurs near Cuautla through springs, wetlands and base flow to the Cuautla River. Deep groundwater circulation through the Cretaceous carbonate rocks discharges towards the spring of Las Estacas (S-32). In addition, local flow systems form in the mountains towards A′ due to topography and contrast of K between the Balsas Group and the limestone aquifer. This suggests that regional discharges near Las Estacas (S-32) possibly mix with local flow systems in the karstic and may explain the reported tritium content (7.4 TU) in this spring (Secretaría de Agricultura y Recursos Hidráulicos (1987); Jaimes-Palomera et al. 1989; Vazquez-Sanchez et al. 1989).

In section BB′ (Fig. 5), the estimated infiltration rate in the Sierra Chichinautzin is close to 50 % of the annual distribution of precipitation. The simulated groundwater flow pattern results in a groundwater divide between the basins of the Amacuzac River and the Basin of Mexico that is displaced with respect to the surface water divide by approximately 9 km towards the Basin of Mexico (Fig. 5); the difference between the surface and subsurface divides is in part due to the difference in topographic elevation of almost 1,000 m between the lowest elevation in the Basin of Mexico and the Amacuzac River in the ARB. This asymmetry results in approximately 75 % of the infiltrated water in the Sierra Chichinautzin flows towards the ARB, while the remaining 25 % flows towards the Basin of Mexico. A similar modeling exercise for the Basin of Mexico by Ortega and Farvolden (1989) estimated that 60 % of the infiltrated water in the Sierra Chichinautzin flows towards the ARB. This difference might be due to the fact that the section utilized by Ortega and Farvolden (1989) did not reach the Amacuzac River, and thus it did not fully include the effect of the elevation difference between the basins. Of the total flux flowing towards the ARB, 73 % of the discharge occurs south of the city of Cuernavaca, between 45 and 55 km from the origin of section BB′. Flux discharging from 56 and 74 km diminishes to 6 %

Table 1 Estimated hydraulic conductivity of the hydrogeologic units in the Amacuzac River Basin

Hydrogeologic unit	K_h (m/day)	Anisotropy ratio K_h / K_v	Porosity
Aquifer in carbonate rocks (HU-1)	1.0	10	0.2
Aquitard, Balsas Group and Mezcala Formation (HU-2)	0.01	10	0.2
Aquitard in Tertiary volcanic rocks (HU-3)	0.005–0.03	5–10	0.15
Aquifer in volcano-sedimentary rocks (HU-4)	2.0–1.0	5	0.25
Aquifer in Quaternary volcanic rocks (HU-5)	0.4	10	0.2
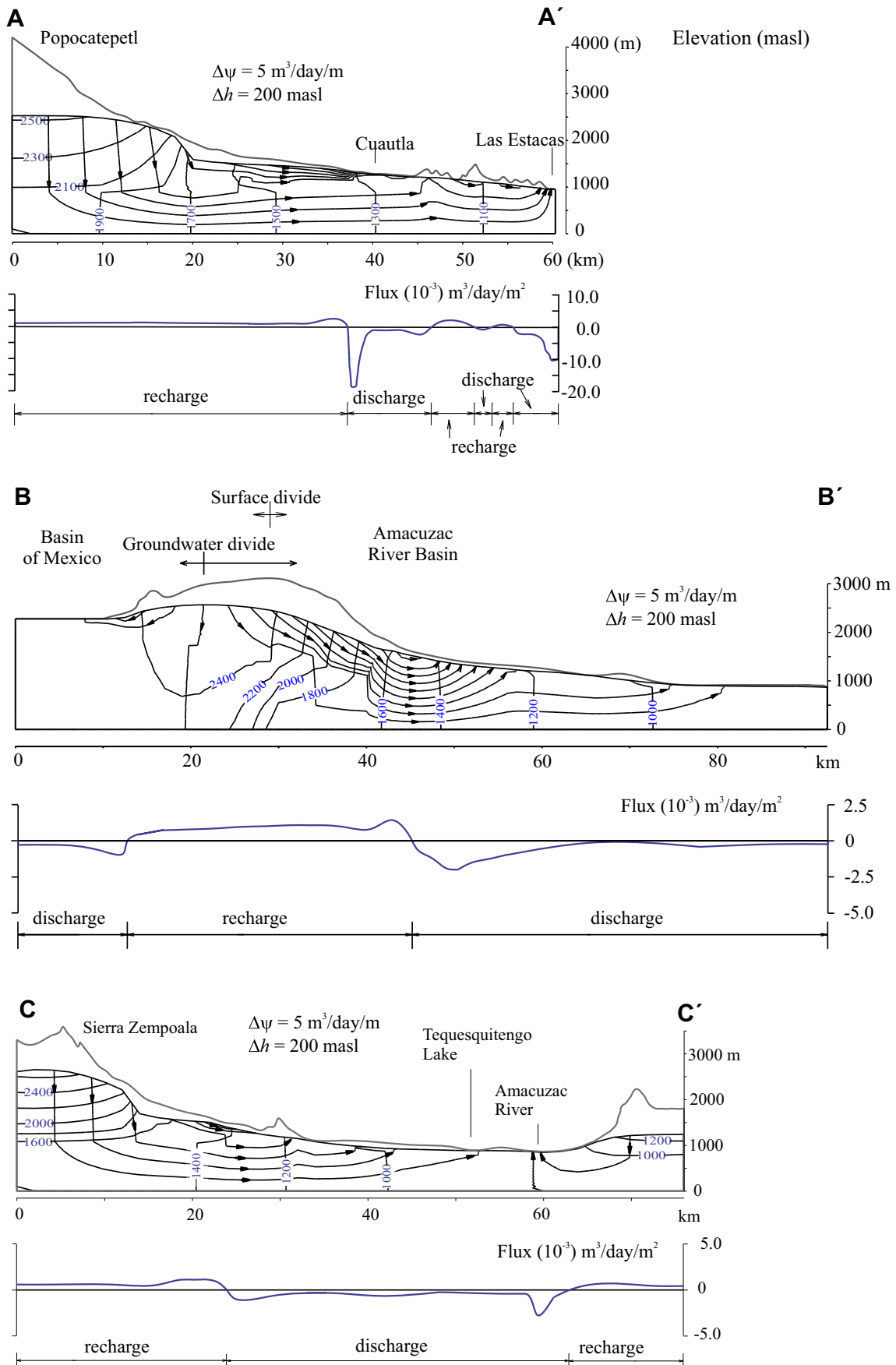
due to the presence of the aquitard HU-2. The remaining 21 % of the flux discharges in the Zacatepec-Jojutla Valley (between 75 and 94 km). Discharge to the Amacuzac River in this section is less than 1.0 m³/day/m².

In section CC' (Fig. 5), estimated recharge in the Sierra Zempoala accounts for 35–40 % of the annual precipitation. Recharge in the Cuernavaca Formation (HU-4) discharges almost immediately as local flow, between 25 and 35 km from the origin of the section, while infiltration in the Sierra Zempoala percolates deeper, reaches the carbonate rocks and discharges in the valley, between 35 and 60 km from the origin of the section. The water table in the mountains was calibrated to about 2,700 masl, consistent with the elevation of the Zictepec spring (with elevation of 2,600 masl).

Residence time

Residence times for flow systems were computed using porosity values estimated for each hydrogeologic unit (Table 1). Local flow systems, for example those discharging in the vicinity of the cities of Cuernavaca and Cuaulta (sections AA′ and BB′, respectively), have residence times ranging from 10 to 500 years; these local flow systems circulate mainly through the hydrogeologic units HU-4 and HU-5 in volcano-sedimentary and Quaternary volcanic rocks. Stream lines reaching deeper to the Cretaceous carbonate rocks and discharging in the middle portion of the valleys have residence time ranging from 600 to 3,000 years. Basin-scale flow systems discharging to the portions with lower elevation in the valleys and to the Amacuzac River have residence time ranging from 4,000 to 10,000 years.

Geochemistry

Main groundwater chemical composition

The results for the chemical analysis of 45 groundwater samples—25 springs (S), 16 wells (W), 3 river water (R) and 1 gallery (G)—are presented in Table 2, where values for major ion concentrations, temperature, pH, TDS and the percent of charge balance error are offered. Figure 6 shows the hydrochemical graphical representation of results through the Stiff diagrams within the ARB. Based on the simulated flow patterns (Fig. 5), the description considers the upper (main groundwater recharge zone), the middle (transition zone) and the lower part (main discharge zone) of the basin. In the upper part of the basin, in the aquifer in Quaternary volcanic rocks (HU-5), which represents the recharge zone

in the Sierra Chichinautzin, groundwater presents very low concentration of ions with a magnesium-calcium-bicarbonate-dominant composition and TDS < 200 mg/L (Fig. 6). Also in this upper part of the ARB, but on Tertiary and Quaternary volcano-sedimentary rocks (HU-4) in the area of Cuautla, groundwater presents a magnesium-bicarbonate-dominant composition and TDS values between 200 and 500 mg/L. Contrasting with this groundwater chemistry, there are two areas in the transition to aquifer in Tertiary and Quaternary volcano-sedimentary rocks (HU-4) and the aquifer in Cretaceous carbonate rocks (HU-1): (1) a sodium-chloride family—Ixtapan (W-17) and Tonatico (S-56)—which increases the TDS to more than 7,000 mg/L, and (2) a calcium-sulfate family (Agua Hedionda (S-21) and Oaxtepec (S-12), which increases the TDS near to 3,000 mg/L. As will be discussed latter, both indicate groundwater flowing through evaporites of different dominant composition.

In the central part of the basin there is a complex distribution of the hydrogeologic units (Fig. 2): the carbonate aquifer (HU-1), the aquitard in the balsas group with gypsum (HU-2), the aquitard in Tertiary volcanic rocks (HU-3) and the aquifer in volcano-sedimentary rocks (HU-4). HU-1 and HU-3 constitute folded rocks and volcanic structures associated to topographic highs, whereas HU-2 and HU-4 are lacustrine deposits and lahar deposits located in the topographic lows. Two samples located along Colotepec-Apatlaco River Valley, Palo Bolero (S-31) and Apotla (W-30), present TDS between 1,800 and 2,000 mg/L with calcium-sulfate dominance (Fig. 6). Whereas, along the Tembembe River, groundwater samples present low concentration of ions with TDS in the range of 400 mg/L (W-26) to 800 mg/L (W-39) with calcium-bicarbonate composition; and along the Yautepec River Valley (W-27, S-32, W-36, W-54) TDS are in the range of 800–1,000 mg/L with calcium-bicarbonate-sulfate composition. South of the Cuautla area, groundwater presents calcium-magnesium-bicarbonate composition and TDS > 800 mg/L (W-33, S-53). The thermal spring of Atotonilco (S-52) located near the easternmost divide of the basin presents a calcium-sulfate composition.

In the lower part of the ARB, the river water samples (R-42 to R-44) present TDS between 450 and 1,050 mg/L of calcium-sulfate-bicarbonate influence. Finally, near the confluence of the Yautepec and Cuautla rivers into the Amacuzac River, near the main discharge zone of the groundwater system (Fig. 5), two springs, S-41 and S-45, present TDS around 2,000 mg/L and a dominant calcium-sulfate composition, probably originated by the evaporitic deposits from the south where the Huitzuco Formation (the lower member of HU-1) with gypsum outcrops. Reported isotopic contents in groundwater from springs 12, 21, 31, 32, 52, and 55 are on average $\delta^{34}S$ $SO_4^{2-} = 16 \pm 0.5$ ‰ and $\delta^{18}O$ $SO_4^{2-} = 14.5 \pm 0.9$ ‰ (Jaimes-Palomera et al. 1989; Vazquez-Sanchez et al.

Table 2 Results of the chemical analyses in groundwater samples

Site No.	Name	Type	UTM E–W	UTM N–S	Elevation (masl)	Temp (°C)	pH	TDS (mg/L)	Ca (meq/L)	Mg (meq/L)	Na (meq/L)	K (meq/L)	HCO_3 (meq/L)	Cl (meq/L)	SO_4 (meq/L)	Charge balance error %
2	Tepoztlán	S	489,700	2,103,000	2,362	18	6.93	126.05	0.82	0.41	0.313	0.097	1.3675	0.275	0.01	-0.38
3	Tlayacapan	W	501,000	2,097,000	1,672	16.4	7.43	79.44	0.84	0.16	0.296	0.041	0.6017	0.425	0.01	12.65
5	Tenancingo	S	438,737	2,095,197	2,038	18.6	7	228.79	1.08	1.47	0.539	0.118	2.5527	0.425	0.031	3.19
6	San Antón	W	473,825	2,092,896	1,584	19.5	6.94	187.35	0.98	1.15	0.539	0.033	2.4615	0.425	0.062	-4.36
7	Sta María	S	472,738	2,097,853	1,863	14.9	6.4	135.87	0.66	0.65	0.313	0.056	1.2308	0.15	0.52	-6.19
8	Laguna Ahuayapan	S	484,239	2,089,092	1,392	14.7	7.33	111.94	0.36	0.72	0.4	0.033	1.094	0.276	0.052	3.10
9	Villa Descanso	W	482,200	2,089,200	1,396	17.9	6.65	287.39	1.15	2.13	0.687	0.097	2.3248	0.69	1	0.61
10	Chalma	S	454,000	2,092,500	1,596	14.9	6.8	120.61	0.82	0.31	0.313	0.056	1.0028	0.138	0.52	-5.12
11	Cocoyoc	W	501,687	2,086,590	1,331	23.3	6.75	523.63	2.13	4.1	1.04	0.097	5.7435	0.425	0.791	2.84
12	Oaxtepec Botánico	S	502,700	2,089,500	1,316	26.1	6.05	2,950.46	24.93	12.46	4	0.251	18.2467	2.76	22.903	-2.65
13	Oaxtepec El Bosque	S	504,600	2,089,800	1,374	18.1	5.62	211.73	1.07	1.14	0.721	0.071	2.3248	0.425	0.004	4.31
15	Las Fuentes	S	482,564	2,087,012	1,347	15.1	7.1	119.16	0.57	0.74	0.383	0.041	1.2308	0.275	0.073	4.69
16	Chapultepec	S	477,990	2,091,235	1,455	16.1	6.42	94.19	0.74	0.16	0.348	0.041	1.2308	0.15	0.031	-4.55
17	Ixtapan	W	428,576	2,084,374	1,918	40.1	6.31	7,352.93	31.2	3.2	67.13	3.1	34.6687	68.31	17.354	-6.98
18	El Sabino	S	506,560	2,082,200	1,345	18.7	6.21	285.18	1.23	1.56	0.696	0.056	3.444	0.276	0.073	-3.42
20	El Bosque	S	504,942	2,082,525	1,341	18.5	5.98	313.06	0.98	2.38	0.757	0.082	3.6	0.552	0.098	-0.60
21	Agua Hedionda	S	507,448	2,080,365	1,333	26.1	6.03	2,832.45	24.85	10.98	4.3	0.235	16.6835	2.138	20.821	0.90
22	El Almeal	S	505,811	2,080,286	1,312	18.1	5.89	312.95	1.48	1.96	0.774	0.082	4.1025	0.414	0.087	-3.46
23	Gpe. Victoria	W	505,441	2,081,843	1,339	18.7	6.07	313.89	0.92	2.36	0.774	0.082	4.1025	0.276	0.087	-3.83
26	Miacatlán	W	463,110	2,075,908	986	26.1	6.96	392.36	2.56	1.24	1.06	0.082	4.6495	0.276	0.167	-1.50
27	Ticumán	W	488,412.7	2,075,237	974	22.6	7.08	926.04	7.13	4.51	1.4	0.128	7.658	0.69	4.165	2.55
28	Chihuahuita	W	480,233	2,073,672	1,132	20.1	6.69	307.84	2.3	1.23	0.722	0.071	3.1908	0.276	0.479	4.56
30	Apotla	W	474,302	2,067,597	1,015	24.2	6.74	1,887.98	19.6	6.96	1.043	0.105	7.025	0.828	19.263	1.08
31	Palo Bolero	S	474,818	2,074,817	1,072	21	6.49	2,004.90	22.88	7.2	0.774	0.087	7.9315	0.828	19.26	4.96
32	Las Estacas	S	487,952	2,071,358	965	22.3	6.96	1,027.69	9.27	3.85	1.4	0.105	6.1993	1.104	7.115	0.71
33	Tenextepango	W	505,001	2,071,362	1,166	23.7	7.12	818.67	4.51	3.77	2.04	0.328	8.211	0.966	1.825	-1.64
34	Mazatepec	W	461,310	2,070,821	1,010	26.9	6.22	649.47	4.2	2.92	1.14	0.159	6.017	1.104	1.9	-3.45
36	Tlaquiltenango	W	481,927	2,062,946	945	23.7	7.02	1,001.25	7.95	5.17	1.31	0.169	6.3863	0.552	6.942	2.52
37	Ojos de Agua	W	463,131	2,061,844	942	25.5	6.97	699.18	6.15	2.71	0.4	0.056	5.5612	0.552	3.6	-2.09
38	Chinameca	W	500,750	2,060,362	1,066	26.5	7.08	854.71	2.97	4.34	4	0.082	8.211	1.38	2.03	-1.00
39	San G. Palmas	W	463,007	2,057,851	922	28.9	7.03	809.68	6.44	4.16	0.26	0.041	6.1082	0.414	4.9	-2.33
41	Tehuixtla 1	S	471,519	2,050,499	866	26.2	6.75	1,924.43	18.12	10.5	0.71	0.082	5.47	0.69	22	2.17
42	Tehuixtla 2	R	471,519	2,050,499	864	30.1	7.95	494.41	3.61	2.05	1.06	0.128	3.7378	0.828	2.3	-0.13
43	Xicatlacotla	R	479,854	2,047,589	789	26.7	7.85	947.25	8.61	3.44	1.217	0.159	4.8318	1.104	7.6	-0.41
44	Tlatenchi	R	480,733	2,055,990	886	28	8	1027.30	9.51	3.69	1.4	0.302	7.111	0.966	5.83	3.45
45	Las Huertas	S	483,870	2,043,163	776	29.4	7.28	2,154.17	20.17	10.25	1.121	0.118	4.7407	0.276	27	-0.56
48	S.P. Zictepec	S	438,870	2,104,680	2,542	15	6.53	214.91	0.82	0.98	0.904	0.082	2.2792	0.414	0.031	1.12
49	Huitzilac	S	471,129	2,104,217	2,607	11.9	6.55	74.28	0.65	0.09	0.252	0.025	0.2735	0.276	0.4	3.43
51	El Túnel	G	475,196	2,094,351	1,620	15.6	6.35	123.06	0.82	0.41	0.33	0.056	1.2308	0.414	0.083	-3.34
52	Atotonilco	S	517,793	2,062,167	1,252	32.8	6.78	1,211.72	11.2	5.28	0.17	0.105	4.9266	0.966	13.013	-6.03
53	Axocoche	S	501,500	2,073,200	1,186	22.8	6.54	1,203.54	7.22	6.97	1.57	0.128	9.3058	0.828	7	-3.77
54	Aqua Splash	W	477,119	2,056,603	930	25.9	6.72	825.10	8.04	1.88	1.51	0.159	7.0198	0.552	3.175	3.77
55	San Ramón	S	479,102	2,077,636	1,191	19.7	6.87	1,176.60	10.99	4.1	0.713	0.071	7.3845	0.138	9	-2.00
56	Tonatico	S	429,717	2,080,327	1,720	36.5	6.13	7,219.24	31.16	6.56	64	2.92	31.9083	67.896	15.941	-5.04
57	Malinalco Truchas	S	447,666	2,093,521	1,665	17.1	6.78	197.30	0.9	0.9	0.6	0.087	2.188	0.414	0.062	-3.44

Notes: *W* well, *S* spring, *R* river, *G* gallery. HCO_3^- measured as total alkalinity in the field. *TDS* computed from chemical analysis

Fig. 6 Stiff diagrams

<table>
</table>
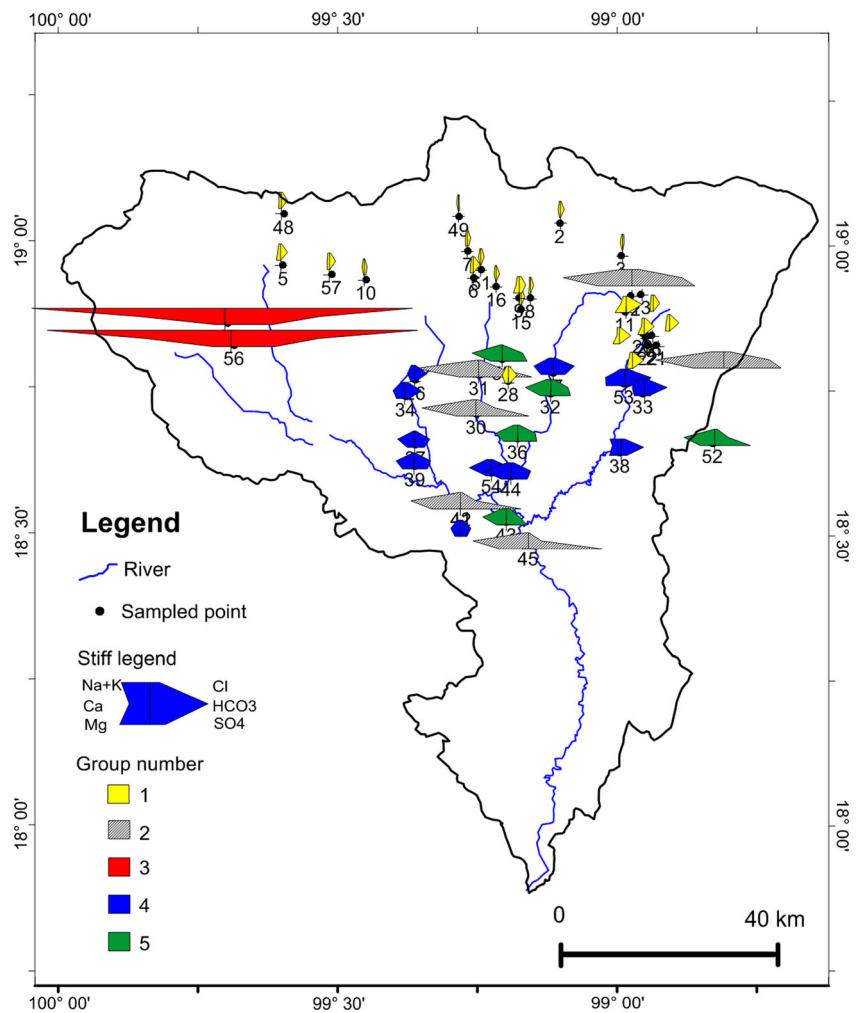
1989) which are consistent with the values of Cretaceous marine evaporites (Claypool et al. 1980). These reported values support gypsum dissolution as the main source of SO_4^{2-} in sulfate-dominated composition of groundwater in the ARB.

From this description, five groups can be defined:

1. Low TDS and magnesium-bicarbonate group at the re-charge zone and short residence time (Chichinautzin and Cuautla).

2. High TDS, between 1,800 and 3,000 mg/L, and calcium sulfate type is observed in (a) the topographic transition with Sierra Chichinautzin reflecting the influence of evaporites, and (b) the middle and lower parts of the ARB, reflecting flow through gypsum.

3. High TDS > 7,000 mg/L, sodium-chloride type, in the topographic transition with Sierra Chichinautzin, westernmost part of the basin, and flows through halite.

4. Low to medium TDS, calcium-bicarbonate type, flows through aquifer in Cretaceous carbonate rocks (HU-1).

Table 3 Loadings and standard deviation of the principal component analysis

	PC1	PC2	PC3
Statistics			
Standard deviation	2.56	1.51	0.89
Proportion of variance	0.68	0.24	0.08
Cumulative proportion	0.68	0.92	1
Loadings			
Elevation	−0.034	0.498	−0.691
Temp	0.315	−0.169	0.461
TDS	0.388	0.051	−0.065
Ca	0.356	−0.212	−0.232
Mg	0.229	−0.484	−0.299
Na	0.341	0.313	0.091
K	0.343	0.304	0.108
HCO_3	0.376	0.066	0.030
Cl	0.338	0.321	0.092
SO_4	0.284	−0.381	−0.365

5. Medium TDS, calcium-bicarbonate-sulfate type, flows through aquifer in Cretaceous carbonate rocks (HU-1) and then Balsas group (HU-2).

Principal component and cluster analyses

The variables included in the PCA are topographic elevation, temperature, TDS and concentration of major ions. A first exploratory PCA resulted in the first three principal components (denoted by PC1, PC2 and PC3) accounting for 96.3 % of the total variance in the data set. After this analysis, only three PCs are retained in the PCA (Table 3) by omitting the rest if their standard deviations are less than or equal to a given value times the standard deviation of the first component. Table 3 also reports the loadings of each of the retained PCs. According to their loadings, PC1 depends of several variables with loadings between 0.3 and 0.4, which suggests PC1 is not associated to a single dominant geochemical process but to two or more processes. PC2 is related to elevation, Mg^{2+} and

SO_4^{2-} with loadings between 0.38 and 0.5; however, three other variables (Cl^-, Na^+ and K^+) have loadings larger than 0.3. Finally, PC3 is mostly related to elevation, temperature and SO_4^{2-} (loadings between 0.69 and 0.36).

Figure 7 depicts the loadings of each variable for the corresponding pair of PCs and plots of scores for PC1 vs. PC2 and PC2 vs. PC3. Colors in Fig. 7 correspond to groups defined in section 'Main groundwater chemical composition'. The plot of PC1 vs. PC2 shows that samples W-17 and S-56 (group 3) depart from the general trend in the ARB followed by the rest of the samples. This general trend is related to elevation, and hence to the length of groundwater flow paths; it is also related to an increase in Mg^{2+}, SO_4^{2-} and, to lesser extent to an increase in Ca^{2+}. This general trend in chemical evolution starts in the positive direction of PC2 where data corresponding to group 1 (recharge zone) are located, whereas groups 4 and 5 (with low to medium TDS and a trend to increase Ca^{2+}, SO_4^{2-} and Mg^{2+}) are located in the negative direction of PC2. The end group of this trend is group 2, with high content of SO_4^{2-} and an increase in Mg^{2+}. It appears then that PC1 vs. PC2 is influenced by (1)
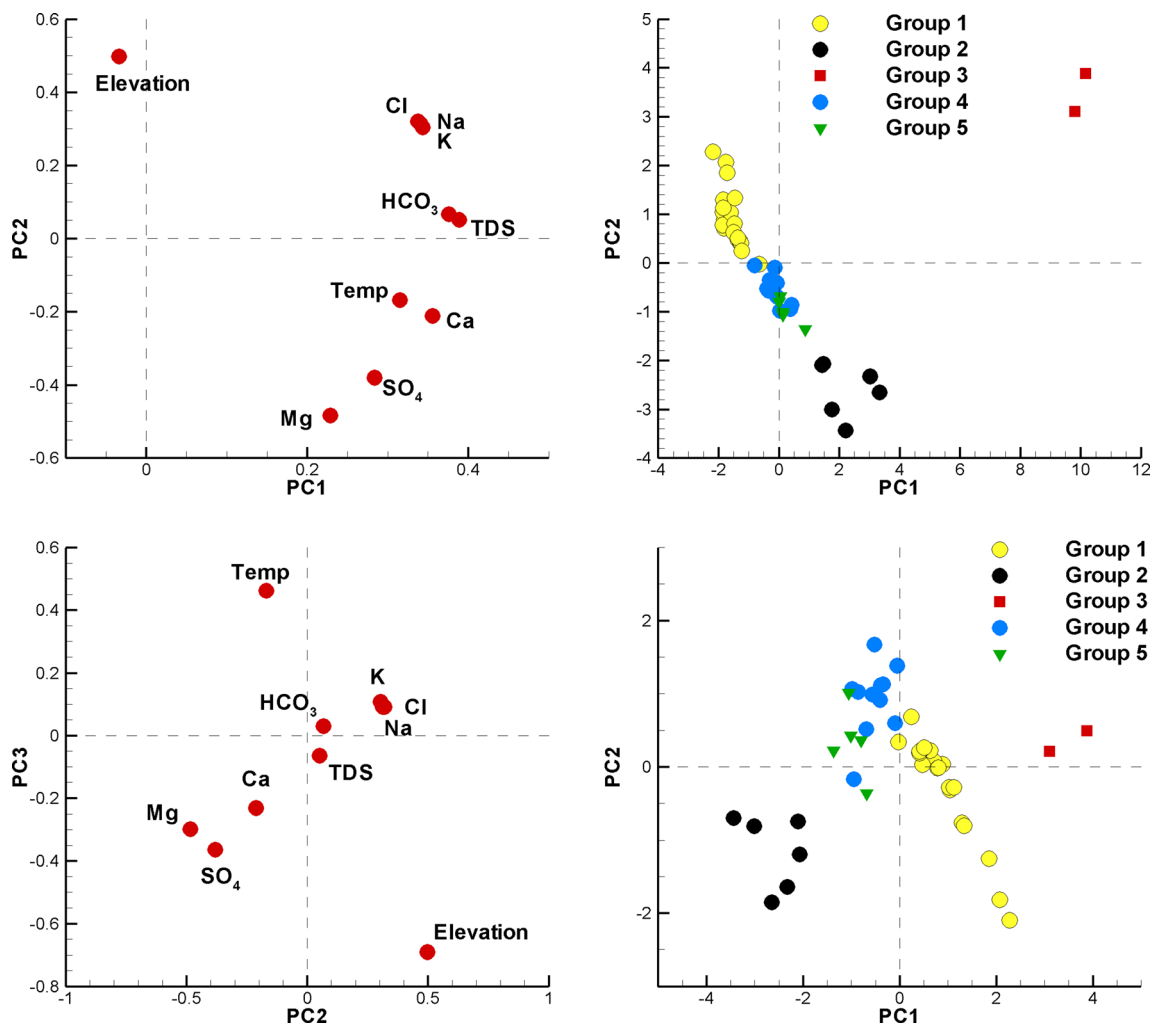

Fig. 7 PCA loadings and scores, for *PC1*, *PC2* and *PC3*

hydrothermal flow through halite (group 3) and (2) a general trend of evolution from recharge zones and then flow through HU-1 and HU-2 (Fig. 5).

A plot of PC2 vs. PC3 (second row in Fig. 7) highlights three different paths from groundwater in the recharge areas (group 1): (1) group 4 roughly continues the trend observed from group 1; (2) group 3 (W-17 and S-56) deviates from this trend, characterized by an increase in Na^+ and Cl^-; (3) groups 5 and 2 also deviate from that trend but to the opposite side of group 3 and they are characterized by high SO_4^{2-} and Mg^{2+} content, probably reflecting dissolution of gypsum.

The PCA scores were then subjected to cluster analysis. Figure 8 depicts the cluster dendrogram for the scores obtained from the PCA. There are four main branches in the dendrogram. These branches are related to the groups defined in section 'Main groundwater chemical composition' and the paths described in the previous paragraph. From left to right, the first branch corresponds to group 1 composed by groundwater in the recharge zone and HU-4 and HU-5. The second branch corresponds to group 3 composed by sodium-chloride samples S-17 and W-56. The third branch corresponds to group 2 composed by calcium-sulfate samples and finally the fourth branch includes groups 4 (calcium-bicarbonate type) and 5 (calcium-bicarbonate-sulfate). There are differences between some of the groups defined by cluster analysis and those formed by chemical family. Samples W-27, W-39, R-44 and S-53 are placed in group 5 by cluster analysis and in group 4 (calcium-bicarbonate type) by inspecting Stiff diagrams, while sample W-11 is placed also in group 4 by cluster analysis and in group 1 from Stiff diagrams. These differences persist if the cluster analysis is repeated excluding temperature, elevation and TDS, i.e., using only major ions as in Stiff diagrams, and are due to the fact that in the cluster analysis a Euclidean distance is computed in the principal component space (accounting for differences and similarities in the chemical composition and additional variables), while the classification from Stiff diagrams is based on the dominant cation–anion composition.

Geochemical modeling

Given the presence of carbonate rocks and gypsum in the ARB, a simulated regional flow pattern where groundwater circulates through those units, a geochemical composition where SO_4^{2-} is the dominant anion in some samples and a regional trend of evolution suggested by the multivariate statistical analysis, geochemical modeling was employed to calculate mineral equilibrium for each of the samples. Table 4 contains the partial pressure of CO_2 (P_{CO2}) and saturation indexes to calcite, aragonite, dolomite, gypsum and anhydrite computed by the code PHREEQE assuming the system is closed to P_{CO2}. Also included in Table 4 are the groups identified from the Stiff diagrams and, when different, the groups obtained by the hierarchical cluster analysis in parenthesis. Figure 9 is a representation of the saturation indexes for calcite, dolomite and gypsum in Table 4 related to molal concentration of SO_4^{2-}, HCO_3^- and elevation. The relation of saturation indexes with mSO_4^{2-} highlights the influence of evaporite rocks on groups 2, 3 and 5, which have gypsum SI from –1 to close to 0 (Fig. 9a). On the other hand, plots of SI versus $mHCO_3^-$ and elevation highlight that groups 1 and 4 represent the general trend of geochemical evolution in the ARB. Groups 1 and 4 form a linear trend when calcite, dolomite and gypsum SIs are plotted versus $mHCO_3^-$ (Fig. 9b). That this trend represents the general geochemical evolution in the ARB is evident when plotting SIs versus elevation (recall that elevation is correlated to some degree with length of flowpath in the regional groundwater flow pattern). In particular for gypsum SI versus elevation, groups 1 and 4 form a trend while groups 2, 3 and to less extent 5, deviate from this trend.

Fig. 8 Cluster dendrogram with selected approximately unbiased probability values (%). Clusters are indicated by *red rounded rectangles* and numbered *1–5*
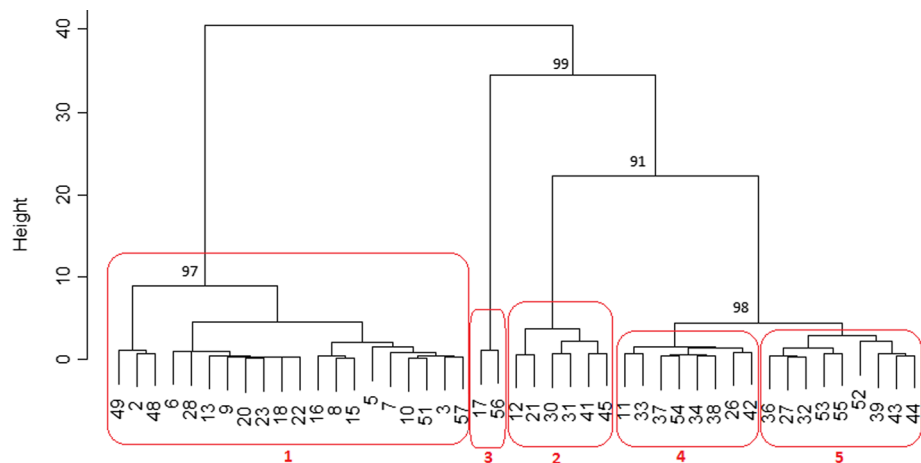
Table 4 Saturation indexes for selected minerals

Group	Site No.	Name	Type	$\log_{10} P_{CO2}$	Calcite	Aragonite	Dolomite	Gypsum	Anhydrite
1	49	Huitzilac	S	−2.23	−2.49	−2.64	−5.90	−2.78	−3.03
1	7	Sta. María	S	1.58	−2.13	−2.28	−4.27	−2.72	−2.97
1	16	Chapultepec	S	−1.68	−2.10	−2.25	−4.85	−3.84	−4.09
1	51	El Túnel	G	−1.53	−2.07	−2.22	−4.43	−3.40	−3.65
1	10	Chalma	S	−2.06	−1.72	−1.87	−3.87	−2.61	−2.86
1	48	S.P. Zictepec	S	−1.42	−1.63	−1.78	−3.18	−3.88	−4.13
1	15	Las Fuentes	S	−2.28	−1.47	−1.62	−2.84	−3.62	−3.87
1	8	Laguna Ahuayapan	S	−2.52	−1.45	−1.61	−2.62	−3.95	−4.20
1	2	Tepoztlán	S	−2.04	−1.39	−1.54	−3.05	−4.32	−4.56
1	57	Malinalco Truchas	S	−1.7	−1.34	−1.49	−2.66	−3.54	−3.79
1	3	Tlayacapan	W	−2.91	−1.25	−1.40	−3.20	−4.28	−4.53
1	6	San Antón	W	−1.89	−1.15	−1.30	−2.17	−3.52	−3.76
1	5	Tenancingo	S	−1.85	−0.97	−1.12	−1.76	−3.80	−4.04
1	9	Villa Descanso	W	−1.53	−1.37	−1.52	−2.43	−2.32	−2.57
1	13	Oaxtepec El Bosque	S	−0.51	−2.39	−2.54	−4.72	−4.68	−4.92
1	20	El Bosque	S	−0.68	−1.91	−2.06	−3.39	−3.39	−3.64
1	22	El Almeal	S	−0.6	−1.83	−1.97	−3.49	−3.27	−3.51
1	23	Gpe. Victoria	W	−0.75	−1.82	−1.97	−3.18	−3.47	−3.71
1	18	El Sabino	S	−0.93	−1.58	−1.73	−3.02	−3.40	−3.64
1	28	Chihuahuita	S	−1.44	−0.86	−1.01	−1.93	−2.35	−2.58
1 (4)	11	Cocoyoc	W	−1.24	−0.60	−0.74	−0.80	−2.28	−2.51
2	21	Agua Hedionda	S	−0.09	−0.06	−0.21	−0.35	−0.31	−0.53
2	12	Oaxtepec Botánico	S	−0.12	−0.06	−0.21	−0.29	−0.29	−0.50
2	31	Palo Bolero	S	−0.9	0.01	−0.13	−0.40	−0.30	−0.53
2	30	Apotla	W	−1.18	0.19	0.05	0.05	−0.35	−0.57
2	45	Las Huertas	S	−1.87	0.59	0.45	1.05	−0.26	−0.46
2	41	Tehuixtla 1	S	−1.29	0.07	−0.07	0.04	−0.35	−0.57
3	56	Tonatico	S	0.08	0.40	0.26	0.36	−0.51	−0.67
3	17	Ixtapan	W	−0.08	0.62	0.49	0.51	−0.47	−0.61
4	26	Miacatlán	W	−1.52	−0.32	−0.46	−0.80	−2.79	−3.00
4	34	Mazatepec	W	−0.67	−0.79	−0.94	−1.59	−1.66	−1.87
4	54	Aqua Splash	W	−1.12	0.00	−0.14	−0.49	−1.22	−1.44
4	37	Ojos de Agua	W	−1.47	0.04	−0.11	−0.15	−1.26	−1.48
4	42	Tehuixtla 2	R	−2.59	0.71	0.57	1.35	−1.60	−1.80
4	33	Tenextepango	W	−1.46	0.20	0.06	0.45	−1.68	−1.91
4	38	Chinameca	W	−1.4	0.02	−0.13	0.35	−1.82	−2.03
4 (5)	39	San G. Palmas	W	−1.47	0.17	0.03	0.33	−1.16	−1.36
4 (5)	27	Ticumán	W	−1.46	0.27	0.13	0.45	−1.20	−1.42
4 (5)	44	Tlatenchi	R	−2.41	1.31	1.16	2.36	−0.98	−1.18
4 (5)	53	Axocoche	S	−0.84	−0.22	−0.37	−0.35	−1.04	−1.26
5	52	Atotonilco	S	−1.37	−0.05	−0.18	−0.23	−0.64	−0.83
5	55	San Ramón	S	−1.29	0.14	−0.01	−0.09	−0.75	−0.99
5	32	Las Estacas	S	−1.44	0.14	−0.01	−0.01	−0.89	−1.12
5	36	Tlaquiltenango	W	−1.48	0.17	0.02	0.26	−0.97	−1.20
5	43	Xicatlacotla	R	−2.42	0.94	0.79	1.62	−0.89	−1.10

Notes: *W* well, *S* spring, *R* river, *G* gallery

Group is defined from Stiff diagrams and cluster analysis (the latter *in parenthesis* if they are different)
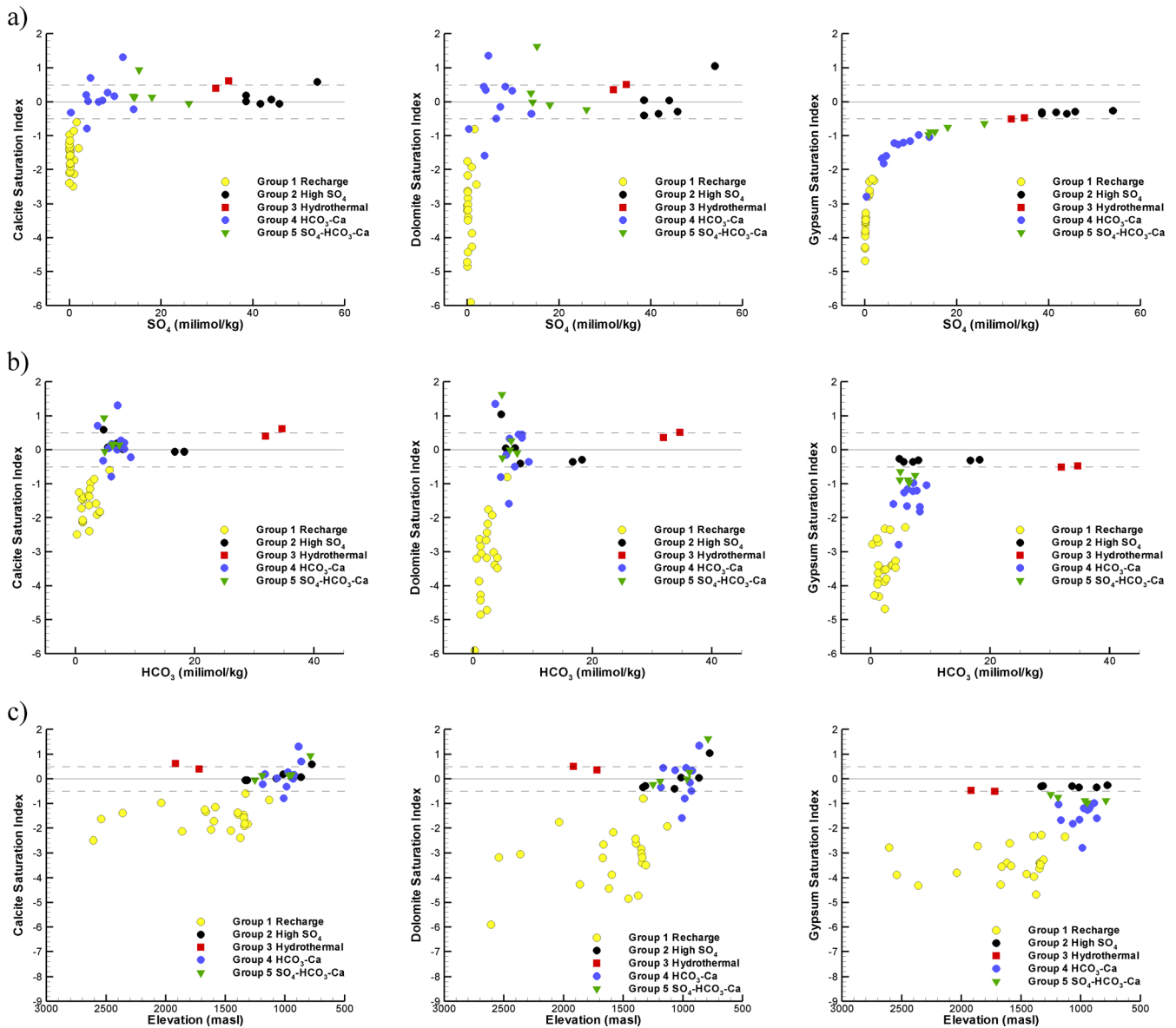
Fig. 9 **a** mSO_4^{2-}, **b** $mHCO_3^-$ and **c** elevation versus saturation index for calcite, dolomite and gypsum. *Horizontal lines* corresponds to SI = 0, while *dashed lines* mark ± 0.5 SI limit

Geochemical processes and groundwater flow

Figure 10 depicts the conceptual model of the groundwater flow and hydrogeochemical evolution in the ARB. At the recharge area in the Quaternary Sierra Chichinautzin, groundwater originates as rain infiltrating through the soil zone and fracture volcanic rocks (HU-5) to the water table. Groundwater movement is through mafic (MgO ≥ 6.0 % wt) and intermediate (MgO ≤ 6.0 % wt) volcanic rocks with abundant phenocrystals and microphenocrystals of olivine, $(Mg, Fe)_2 SiO_4$, and less abundant pyroxene—most common form $(Ca,Mg,Fe)_2Si_2O_6$—hornblende and plagioclase ($NaAlSi_3O_8$ to $CaAl_2Si_2O_8$ series; Meriggi et al. 2008). The movement of groundwater (Fig. 5) interacts with different minerals of these

volcanic rocks increasing the concentration of bicarbonate from potential dissolution of plagioclase and Mg^{2+} and Ca^{2+} from olivine and also from plagioclases (Fig. 6). Figure 6 shows a lower ion concentration and a dominant bicarbonate-calcium-magnesium composition associated to dissolution of volcanic minerals.

Below the aquifer in Quaternary volcanic rocks (HU-5), groundwater paths continue as shallow and deeper flows, the first though Quaternary and Tertiary volcanic and volcano-sedimentary rocks (HU-5 and HU-4) and the second through the aquifer in Cretaceous carbonate rocks (UH-1; Figs. 5 and 10). The shallow groundwater in the Cuautla area contains evidence that the water flows through specific volcanic mineral phases along its flow path, with small but progressive
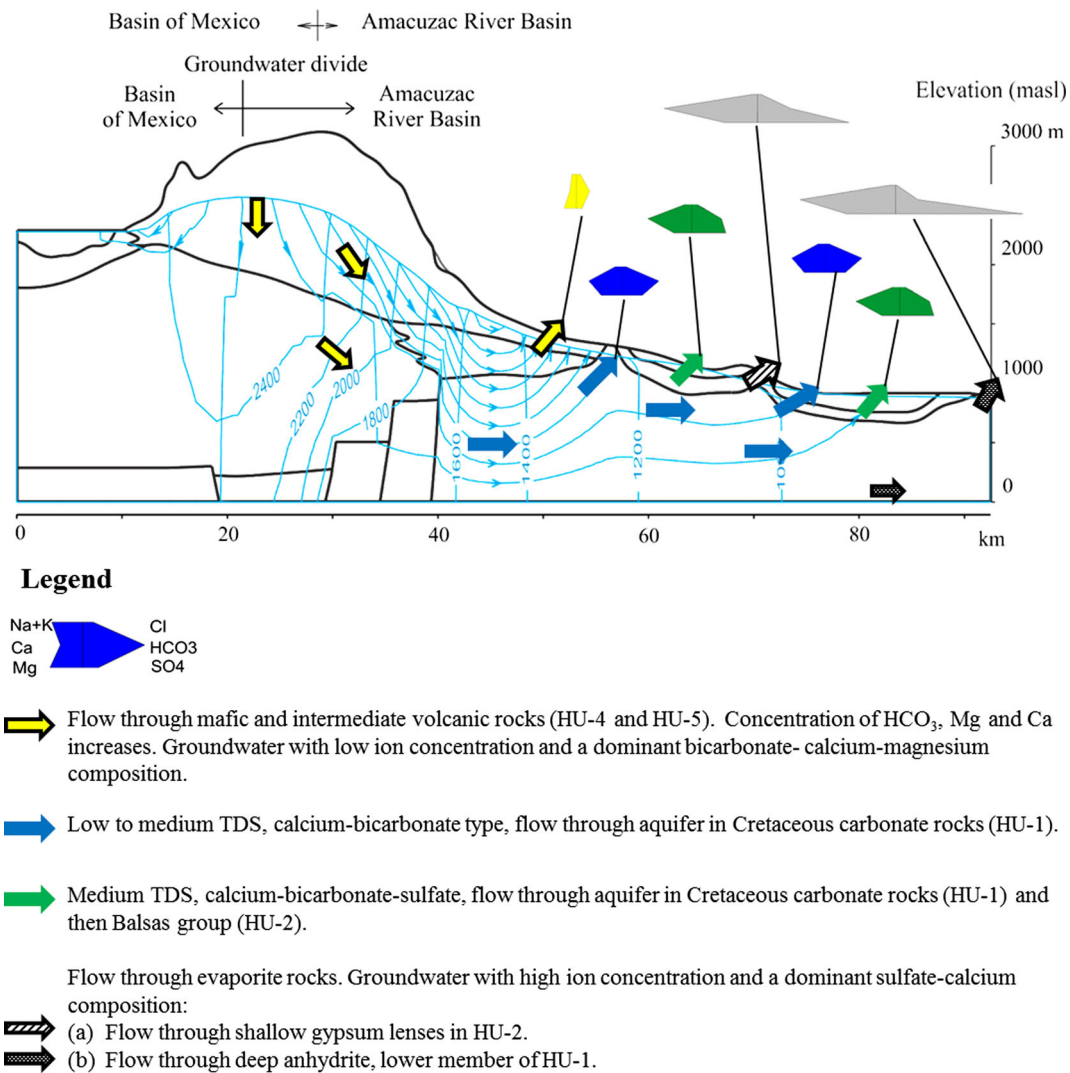
Legend

Flow through mafic and intermediate volcanic rocks (HU-4 and HU-5). Concentration of HCO_3, Mg and Ca increases. Groundwater with low ion concentration and a dominant bicarbonate- calcium-magnesium composition.

Low to medium TDS, calcium-bicarbonate type, flow through aquifer in Cretaceous carbonate rocks (HU-1).

Medium TDS, calcium-bicarbonate-sulfate, flow through aquifer in Cretaceous carbonate rocks (HU-1) and then Balsas group (HU-2).

Flow through evaporite rocks. Groundwater with high ion concentration and a dominant sulfate-calcium composition:
(a) Flow through shallow gypsum lenses in HU-2.
(b) Flow through deep anhydrite, lower member of HU-1.

Fig. 10 Conceptual model of groundwater flow and hydrogeochemical evolution in the ARB (hydrostratigraphy depicted in Fig. 4); size of Stiff diagrams is proportional to total dissolved solids (TDS); flow lines are marked with *arrows* and equipotentials are labeled by its value

increases of magnesium-calcium and bicarbonate in solution (group 1; Fig. 5). Figure 10 shows that the deeper flow encounters the aquitard (HU-3) and the carbonate aquifer (HU-1). In the latter, as the water passes through the limestones, under closed conditions with respect to CO_2, dissolution of calcite occurs (increasing contents of Ca, HCO_3 and values of calcite SI). Based on the presence of sinkholes (Tequesquitengo, Coatetelco and El Rodeo, Fig. 1) in the discharge zone, apparently groundwater did not get saturated with calcite, thereby potentially dissolving the calcite until the collapse of the structure occurred. The lakes are fed by groundwater (De la O-Carreño 1954). However, when groundwater encounters thick gypsum lenses in HU-2 (depicted as arrows with diagonal lines in Fig. 10) or the Huitzuco anhydrite, which is the lower member of HU-1 (flow depicted by black arrows in Fig. 10), more calcium and sulfate enter into solution and causes supersaturation with respect to calcite as observed for samples in group 2 (Fig. 9);

consecutive precipitation of calcite may occur, causing undersaturation with respect to gypsum, and then more dissolution of gypsum near to saturation (group 2). When gypsum content in HU-2 is small, groundwater acquires a predominant sulfate-calcium composition but with lesser TDS content than the previous case (group 5, green arrows in Fig. 10). Groundwater flow through halite and possibly hydrothermal influence with high TDS (>7,000 mg/L) and sodium-chloride composition are not depicted in Fig. 10 because these characteristics are limited to two samples in the western portion of the ARB.

Conclusions

Groundwater flow and hydrogeochemistry, in the Amacuzac River Basin, have been studied using both finite element cross-sectional flow and equilibrium geochemical modeling,

supported by a multivariate statistical analysis. A traditional gravity groundwater-flow system is produced by the model, showing the main features of the flow system and supporting the results of hydrogeochemical investigations.

Groundwater recharge in the mountains is calculated as between 35 and 50 % of the distribution of the average precipitation. Hydraulic conductivities of the six hydrogeologic units used in the model, were obtained from the best available sources and from field observations of the rocks and runoff characteristics from values cited in the literature and adjusted during the modeling.

Of the total flux flowing towards the Amacuzac River Basin, about 73 % of the discharge occurs south of the city of Cuernavaca, in the upper third of the basin; 6 % of the discharge occurs in the middle of the basin, due to the presence of the aquitard HU-2; and the remaining 21 % of the flux discharges in the Zacatepec-Jojutla Valley.

Residence times for the local flow systems, in the volcano-sedimentary aquifer (HU-4) and Quaternary volcanic rocks (HU-5), range from 10 to 500 years. Stream lines reaching deeper to the Cretaceous carbonate rocks (HU-1) and discharging in the middle portion of the valleys have residence times ranging from 600 to 3,000 years; whereas, regional flow systems have residence times ranging from 4,000 to 10,000 years.

The predominant groundwater reactions in the Amacuzac River Basin are influenced by the order in which the various igneous and sedimentary rocks are encountered by the groundwater flow and the prevailing closed conditions to P_{CO2} in the system, consistent with the principal component and cluster analysis: (1) recharge water in the volcanic and volcano-sedimentary aquifers increases the concentration of bicarbonate from potential dissolution of plagioclase and Mg^{2+} and Ca^{2+} from olivine and also from plagioclases, (2) deeper groundwater flow encounters carbonate rocks, under closed conditions with respect to CO_2, and dissolves calcite and dolomite, (3) when groundwater encounters thick shallow gypsum lenses in HU-2 or the deeper Huitzuco anhydrite (lower member of HU-1) gypsum dissolution produces increased concentrations of Ca^{2+} and SO_4^{2-}, (4) two samples reflected the influence of hydrothermal fluids and probably halite dissolution present in evaporitic deposits.

References

Aguilera-Franco N (2003) Cenomanian–Coniacian zonation (foraminifers and calcareous algae) in the Guerrero-Morelos basin, southern Mexico. Rev Mexicana Ciencias Geol 20(3):202–222

Bendig GL (1995) Regional assessment of contamination susceptibility and possible protection strategies for the groundwater resources of the valley of Cuernavaca, Morelos, Mexico. MSc Thesis, University of Waterloo, Waterloo, ON, Canada

Christophersen N, Hooper RP (1992) Multivariate analysis of stream water chemical data: the use of principal components analysis for the end-member mixing problem. Water Resour Res 28(1):99–107

Claypool GE, Holser WT, Kaplan IR, Sakai H, Zak I (1980) The age curves of sulfur and oxygen isotopes in marine sulfate and their mutual interpretation. Chem Geol 28:199–260

Comisión Nacional del Agua (1989) Proyecto Oacalco (Oacalco project). Technical report. Comisión Nacional del Agua, Mexico City

CONAGUA (2015) Disponibilidad del agua subterránea (d.o.f. 20 de abril de 2015) [Availability of groundwater (20 April 2015)]. http://www.conagua.gob.mx/disponibilidad.aspx?n1=3&n2=62&n3=112. Accessed November 2015

De La O-Carreño (1954) Las provincias geohidrologicas de Mexico [Geohydrological provinces of Mexico]. Boletín 56 del Instituto de Geología, Instituto de Geología, Mexico City, 2 volumes

DeCerna Z, Ortega-Gutiérrez F, Palacios-Nieto M et al. (1980) Reconocimiento geológico de la parte central de la cuenca del alto Río Balsas, Estados de Guerrero y Puebla [Geologic recognizance of the central part of the upper Balsas River, states of Guerrero and Puebla]. In: Libro guía de la excursión geológica a la cuenca del alto Río Balsas. Sociedad Geológica Mexicana, Mexico City, pp 1–33

Deming D, Nunn JA (1991) Numerical simulations of brine migration by topographically driven recharge. J Geophys Res 96(B2):2485–2499

Everitt BS, Hothorn T (2010) A handbook of statistical analyses using R, 2nd edn. CRC, Boca Raton, FL

Forster C, Smith L (1988a) Groundwater flow systems in mountainous terrain: 1, numerical modeling technique. Water Resour Res 24(7):999–1010

Forster C, Smith L (1988b) Groundwater flow systems in mountainous terrain: 2, controlling factors. Water Resour Res 24(7):1011–1023

Freeze RA, Witherspoon PA (1966) Theoretical analysis of regional groundwater flow: 1, analytical and numerical solutions to the mathematical model. Water Resour Res 2(4):641–656

Freeze RA, Witherspoon PA (1967) Theoretical analysis of regional groundwater flow: 2, effect of water-table configuration and subsurface permeability variation. Water Resour Res 3(2):623–634

Freeze RA, Witherspoon PA (1968) Theoretical analysis of regional ground water flow: 3, quantitative interpretations. Water Resour Res 24(3):581–590

Fries CJ (1960) Geología del estado de Morelos y de partes adyacentes de México y Guerrero, región central meridional de México [Geology of the State of Morelos and parts of Mexico and Guerrero, central meridional región of Mexico]. Boletín 60 del Instituto de Geología, Universidad Nacional Autónoma de México, Mexico City

Fries CJ (1965) Hoja geológica Cuernavaca y Resumen de la geología, estados de Morelos, Puebla y Guerrero [Geologic map Cuernavaca and summary of the geology, states of Morelos, Puebla and Guerrero]. Instituto de Geología, Universidad Nacional Autónoma de México, Mexico City

Frind EO, Matanga GB (1985) The dual formulation of flow for contaminant transport modeling: 1, review of theory and accuracy aspects. Water Resour Res 21(2):159–169

Garven G (1995) Continental-scale groundwater flow and geologic processes. Ann Rev Earth Planet Sci 23:89–117

Garven G, Freeze RA (1984a) Theoretical analysis of the role of groundwater flow in the genesis of stratabound ore deposits: 1, mathematical and numerical model. Am J Sci 284(10):1085–1124

Garven G, Freeze RA (1984b) Theoretical analysis of the role of groundwater flow in the genesis of stratabound ore deposits: 2, quantitative results. Am J Sci 284(10):1125–1174

Garven G, Ge S, Person MA, Sverjensky DA (1993) Genesis of stratabound ore deposits in the midcontinent basins of North

America: 1, the role of regional groundwater flow. Am J Sci 293(6): 497–568

Ghasemizadeh R, Yu X, Butscher C, Hellweger F, Padilla I, Alshawabkeh A (2015) Equivalent porous media (EPM) simulation of groundwater hydraulics and contaminant transport in karst aquifers. PLoS ONE 10(9):e0138954. doi:10.1371/journal.pone.0138954

Hernández-Romano U, Aguilera-Franco N, Martínez-Medrano M, Barceló-Duarte J (1997) Guerrero-Morelos Platform drowning at the Cenomanian-Turonian boundary, Huitziltepec area, Guerrero State, southern Mexico. Cretac Res 18(5):661–686

Hooper RP (2009) Diagnostic tools for mixing models of stream water chemistry. Water Resour Res 39(3):HWC21–HWC213. doi:10.1029/2002WR001528

Jaimes-Palomera LR, Cortes-Silva A, Vazquez-Sanchez E, Aravena R, Fritz P, Drimmie R (1989) Geoquímica isotópica del sistema hidrogeológico del valle de Cuernavaca, Estado de Morelos, México [Isotopic geochemistry of the hydrogeologic system in the Cuernavaca Valley, Morelos State, Mexico]. Geofís Int 28(2):219–244

Jamieson GR, Freeze RA (1983) Determining hydraulic conductivity distribution in a mountainous area using mathematical modeling. Ground Water 21(2):168–177

Laaksoharju M, Skårman C, Skårman E (1999) Multivariate mixing and mass balance (M3) calculations, a new tool for decoding hydrogeochemical information. Appl Geochem 14(7):861–871

Long AJ, Valder JF (2011) Multivariate analyses with end-member mixing to characterize groundwater flow: wind cave and associated aquifers. J Hydrol 409(1–2):315–327

Long JCS, Remer JS, Wilson CR, Witherspoon PA (1982) Porous media equivalents for networks of discontinuous fractures. Water Resour Res 18(3):645–658. doi:10.1029/WR018i003p00645

McLaren RG (1988) CROSSFLO, a 2-D steady state flow in cross section. Waterloo Center for Groundwater Research, Univ. of Waterloo, Waterloo, ON

Meriggi L, Macías JL, Tommasini S, Capra L, Conticelli S (2008) Heterogeneous magmas of the Quaternary Sierra Chichinautzin volcanic field (central Mexico): the role of an amphibole-bearing mantle and magmatic evolution processes. Rev Mexicana Ciencias Geol 25(2):197–216

Niedzielski H (1994) Características del manantial "Las Estacas" en Morelos, México [Characteristics of "Las Estacas" spring in Morelos, Mexico]. Geof Int 33(2):283–294

Nieto-Samaniego AF, Alaniz-Alvarez SA, Silva-Romo G, Equiza-Castro MH, Mendoza-Rosales CC (2006) Latest Cretaceous to Miocene deformation events in the eastern Sierra Madre del Sur, Mexico, inferred from the geometry and age of major structures. Bull Geol Soc Am 118(1-2):238–252

Ortega A, Farvolden RN (1989) Computer analysis of regional groundwater flow and boundary conditions in the Basin of Mexico. J Hydrol 110(3–4):271–294

Ortega-Guerrero A (2003) Origin and geochemical evolution of groundwater in a closed-basin clayey aquitard, northern Mexico. J Hydrol 248(1-4):26–44

Palmer CD, Cherry JA (1984) Geochemical evolution of groundwater in sequences of sedimentary rocks. J Hydrol 75(1-4):27–65

Parkhurst DL, Thorstenson DC, Plummer LN et al (1980) PHREEQE: a computer program for geochemical calculations. US Geol Surv Water Resour Invest Rep 80-96

Pearson M, Raffensperger JP, Ge S, Garven G (1996) Basin-scale hydrogeologic modeling. Rev Geophys 34(1):61–87

Scanlon BR, Mace RE, Barrett ME, Brian Smith B (2003) Can we simulate regional groundwater flow in a karst system using equivalent porous media models? Case study, Barton Springs Edwards aquifer, USA. J Hydrol 276:137–158

Secretaría de Agricultura y Recursos Hidráulicos (1981a) Estudio geohidrológico preliminar de la zona de Cuautla-Yautepec, Morelos, Mexico [Preliminar geohydrologic study of the Cuautla-Yautepec area, Morelos, Mexico]. Technical report, Secretaría de Agricultura y Recursos Hidráulicos, Mexico City

Secretaría de Agricultura y Recursos Hidráulicos (1981b) Estudio geohidrológico preliminar del Valle de Cuernavaca, en el estado de Morelos, Mexico [Preliminar geohydrologic study of the Valley of Cuernavaca, Morelos State, Mexico]. Technical report, Secretaría de Agricultura y Recursos Hidráulicos, Mexico City

Secretaría de Agricultura y Recursos Hidráulicos (1981c) Estudio geohidrológico preliminar del valle de Zacatepec, estado de Morelos, Mexico [Preliminary geohydrologic study of the Valley of Zacatepec, Morelos State, Mexico]. Technical report, Secretaría de Agricultura y Recursos Hidráulicos, Mexico City

Secretaría de Agricultura y Recursos Hidráulicos (1987) Análisis de flujo de agua subterránea del Valle de México mediante trazadores isotópicos [Groundwater flow analysis of the Valley of Mexico via isotopic tracers]. Technical report, Instituto de Geofísica, UNAM, Mexico City

Stuyfzand P (1999) Patterns in groundwater chemistry resulting from groundwater flow. Hydrogeol J 7(1):15–27

Suk H, Lee KK (1999) Characterization of a ground water hydrochemical system through multivariate analysis: clustering into ground water zones. Ground Water 37(3):358–366

Suzuki R, Shimodaira H (2006) Pvclust: an R package for assessing the uncertainty in hierarchical clustering. Bioinformatics 22(12):1540–1542

Tóth J (1963) A theoretical analysis of groundwater flow in small basins. J Geophys Res 68(16):4795–4812

Tóth J (1995) Hydraulic continuity in large sedimentary basins. Hydrogeol J 3(4):4–16

Tóth J (1999) Groundwater as a geologic agent: an overview of the causes, processes, and manifestations. Hydrogeol J 7(1):1–14

Varni M, Carrera J (1998) Simulation of groundwater age distributions. Water Resour Res 34(12):3271–3281

Vazquez-Sanchez E, Cortes A, Jaimes-Palomera R, Fritz P, Aravena R (1989) Hidrogeología isotópica de los valles de Cuautla y Yautepec, México [Isotopic hydrogeology in the valleys of Cuautla and Yautepec, Mexico]. Geofís Int 28(2):245–264

Ward JH (1963) Hierarchical grouping to optimize an objective function. J Am Stat Assoc 58(301):236–244

Weissmann GS, Zhang Y, LaBolle EM, Fogg GE (2002) Dispersion of groundwater age in an alluvial aquifer system. Water Resour Res 38(10):1198. doi:10.1029/2001WR000907